

Using Flexible Trapezoidal Quad-Surfaces for Transformable Design

Kiumars SHARIFMOGHADDAM*, Georg NAWRATIL,
Arvin RASOULZADEH, Jonas TERVOOREN

*Institute of Discrete Mathematics and Geometry, TU Wien
Center for Geometry and Computational Design, TU Wien
ksharif@geometrie.tuwien.ac.at

Abstract

Generic discrete surfaces composed of quadrilateral plates connected by rotational joints in the combinatorics of a square grid are rigid, but their also exist special ones with a 1-parametric flexibility. We focus on the particular class of so-called T-hedra, which can be thought as a generalization of discrete surfaces of revolution in such a way that the axis of rotation is not fixed at one point but rather sweeping a polyline path on the base plane. Moreover, the action does not need to be a pure rotation but can be combined with an axial dilatation. After applying these transformations to the breakpoints of a certain discrete profile curve, a flexible quad-surface with planar trapezoidal faces is obtained. Therefore, the design space of T-hedra also includes as subclasses discretized translational surfaces and molding surfaces beside the already mentioned rotation surfaces. We provide a Rhino/Grasshopper plugin developed with C#, which makes the design space of T-hedra accessible for designers and engineers. Our components enable the user to design a T-hedron interactively and visualize its deformation in real-time based on a recursive parametrization of the quad-mesh vertices under the associated isometric deformation. Furthermore, there is an interesting option to evaluate the force transmission characteristic within the surface by considering each four planes with a common node as a spherical 4-bar linkage.

Keywords: quad-mesh, discrete surface, Rhino/Grasshopper, isometric deformation, transformable design, flexible quad-surfaces, C#, interactive design, T-hedron

1. Introduction

Since Chuck Hoberman's pioneering work [1] on transformable design, the interest in this topic has increased due to applications in engineering (e.g. transformable structures [2]), robotics (e.g. deployable mechanisms [3]), material sciences (e.g. reconfigurable metamaterials [4]), medicine (e.g. auxetic stents [5]), etc. In architectural applications one puts great value not only on the functionality but also on the aesthetic appearance; e.g.

- transformable facade/roof elements under functional aspects of ventilation and shading/lighting [6,7] or
- adaptive ceilings and wall coverings under functional aspects of acoustics [8,9].

A particular class of transformable surfaces is composed of quadrilateral plates connected by rotational joints in the combinatorics of the square grid. During the motion of these so-called flexible quad-surfaces, no elastic or plastic deformations of panels are allowed, only hinge rotations. The degrees-of-freedom (dofs) count shows that a generic quad-surface is rigid. Hence, the special quad-surfaces that are flexible typically have one dof: the complete spatial shape is controlled by a single dihedral angle

between hinged panels. This behavior of quad-surfaces stands in contrast to surfaces made of triangular panels, which have several dofs, and whose motion is harder to control.

1.1. Review

It is known [10] that a quad-surface is flexible if and only if every 3×3 complex (Fig. 1, left) is flexible. Such complexes are often called Kokotsakis polyhedra due to Kokotsakis [11], who found necessary and sufficient conditions for their infinitesimal flexibility. Based on spherical kinematics [12], a partial classification of flexible 3×3 complexes was obtained by Stachel and Nawratil [13-15]. Inspired by this approach Izmistiev [16] obtained a full classification containing more than 20 cases. Recently, it was shown [17] that Stachel's conjecture holds true, that all flexible 3×3 complexes rely on reducible compositions of two spherical four-bar linkages.

To the present day, the only computational design method for flexible quad-surfaces is the one of Tachi (e.g. [18,19]). This tool uses combinations of special discrete Voss surfaces (Fig. 1, right), which were first studied by Sauer and Graf [20] in 1931 under the name of V-hedra (V-Flache in German). In the same publication [20] also the so-called T-hedra (T-Flache in German) were introduced. In contrast to general flexible quad-surfaces (cf. [16]), T-hedra allow direct access to their spatial shape. This is the base for the developed design tool presented in this paper, which is structured as follows.



Figure 1: (left) 3×3 complex. (right) Two configurations of a flexible model of a V-hedron [21].

1.2. Outline

In Section 2, we summarize from [20,22] the synthetic geometric description of T-hedra and their flexion, which is the base for a recursive parametrization of their vertices under the associated isometric deformation given in Section 3. These precise theoretical computations are used for the Rhino/Grasshopper plugin presented in Section 4, which makes the design space of T-hedra accessible for designers and engineers. Our C# scripted components enable the user to design a T-hedron interactively and to visualize and evaluate its deformation in real-time. Finally, the paper is concluded in Section 5.

2. Geometry of T-hedra

In the following we give the explicit geometric construction of T-hedra and the reasoning for their flexibility, as these already known facts are only available in German-language literature until now (cf. [20,22]).

2.1. Synthetic construction

We start with a planar polygon p_0 located in the plane π_0 and a planar polygon t_0 whose carrier plane is denoted by τ_0 . Moreover, p_0 and t_0 have a common vertex $V_{0,0}$ and the planes π_0 and τ_0 are orthogonal to each other (see Fig. 2, left). The remaining vertices of t_0 and p_0 are denoted by $V_{i,0}$ and $V_{0,j}$, respectively, with $i = 1, \dots, I - 1$ and $j = 1, \dots, J - 1$. Through each vertex $V_{i,0}$ of t_0 there is a plane π_i orthogonal to τ_0 and the resulting set of planes envelopes a so-called guiding prism Γ whose intersection with the plane τ_0 yields the prism polygon g .

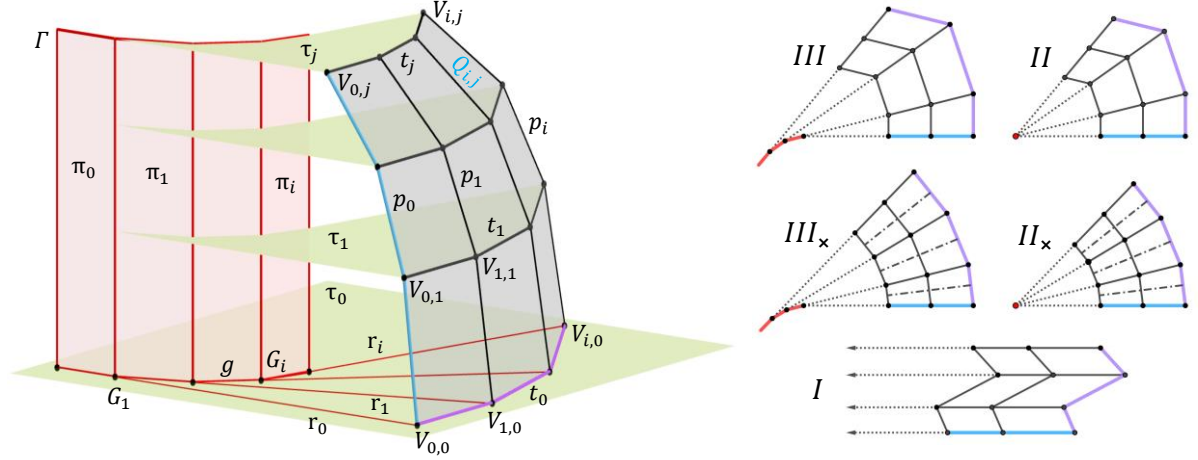


Figure 2: (left) Geometric construction of a T-hedron. (right) Classification of T-hedra based on their top views.

By a parallel projection η_i of p_{i-1} into the plane π_i along the direction of the polygon edge $V_{i-1,0}V_{i,0}$ of t_0 , we obtain the planar polygon $p_i \in \pi_i$. Under this projection the vertices $V_{i-1,j}$ are mapped to $V_{i,j}$. Iteration of this process (for $i = 1, \dots, I - 1$) generates the vertices of the quad-mesh, which has planar trapezoidal faces as the sides $V_{i-1,j-1}V_{i,j-1}$ and $V_{i-1,j}V_{i,j}$ of every quad $Q_{i,j}$ are parallel (due to η_i). This reasons the nomenclature T-hedron.

By connecting the vertices $V_{0,j}, V_{1,j}, \dots, V_{I-1,j}$, we obtain polygons t_j in planes τ_j parallel to τ_0 . The polygons t_j and planes τ_j are also known as trajectory polygons/planes (t-polygons/planes) and the polygons p_i and planes π_i are named profile polygons/planes (p-polygons/planes). Moreover, the quad strips enclosed by two neighbouring t/p-polygons are called trajectory/profile strips (t/p-strips).

2.2. Subclasses

In general, the mapping η_i implies that p_{i-1} and p_i are related by an affinity, which can specialize to a congruence transformation. Moreover, the guiding prism Γ can degenerate into a (finite or ideal) line l . With respect to these two criteria one can classify the set of T-hedra as follows (Fig. 2, right):

- Profile-affine T-hedra (the arms of a trapezoid differ in length)
 - Guiding prism does not degenerate: Type III (most general case)
 - Guiding prism degenerates into a finite line: Type II
- Profile-congruent T-hedra (the arms of a trapezoid have the same length)
 - Guiding prism degenerates into an ideal line: Type I
 - Guiding prism does not degenerate: Type III_x (special case of type III)
 - Guiding prism degenerates into a finite line: Type II_x (special case of type II)

Remark 1: Note that for types II_x and III_x each trapezoid is an isosceles one and for type I all trapezoids degenerate into parallelograms. For computational reasons (cf. Sections 3 and 4) the numbering of the classification differs from those done in [20] and [22], which are also not consistent.

Alternatively, to the mapping η_i , the polygon p_i can be generated from p_{i-1} by a

- ad I. Translation
- ad II. Composition of a rotation and an axial dilatation with axis l
- ad III. Composition of a rotation and an axial dilatation with axis $\pi_{i-1} \cap \pi_i$ of Γ

If the scaling factor of the axial dilatation is constant one, then we get as special cases II_x and III_x, respectively. This shows that the set of T-hedra contains discretized translational surfaces (type I), rotation surfaces (type II_x) and molding surfaces (type III_x).

Remark 2: Note that for type II (and its special case II_x) the t -polygons are related by a central similarity. For type I they are even congruent.

2.3. Isometric deformation

Theorem 13.1 of [22]: A T -hedron allows a 1-parametric set of continuous isometric deformations into T -hedra, which are of the same type as the original T -hedron.

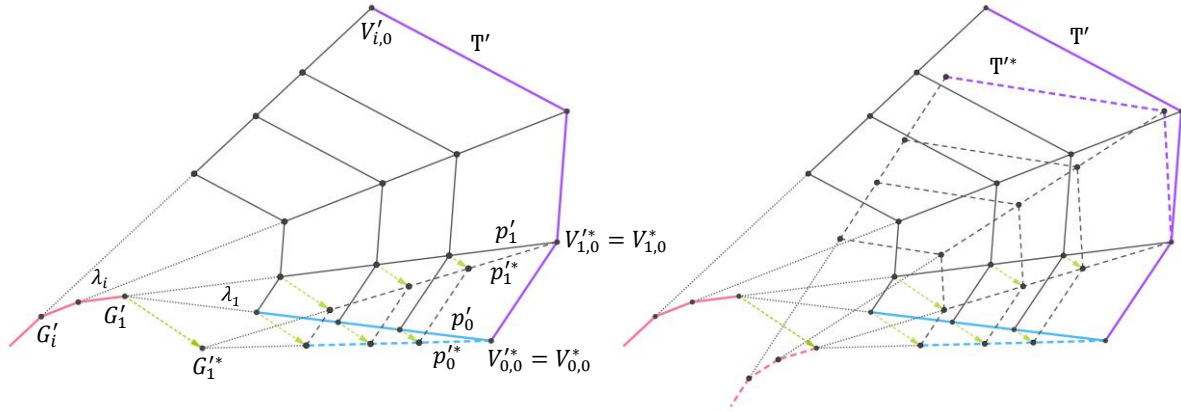


Figure 3: (left) Top view of the given T -hedron including the orthogonal affinity of the first strip (dashed lines). (right) Top view of the given T -hedron and the deformed T -hedron (dashed lines).

Proof: We project the T -hedron T orthogonal onto the plane τ_0 . The resulting top view figure is denoted by T' . In the following we show that there exists a continuous 1-parametric deformation of T' such that the deformed figure T'^* can be seen as the top view of another T -hedron T^* , which results from T by a continuous isometric deformation.

Deforming T' into T'^* : For each p -strip of T' we consider the affine transformation orthogonal to the parallel sides of the trapezoids. For the first strip bounded by p'_0 and p'_1 (cf. Fig. 3, left) the related distortion factor d can be chosen arbitrary within some certain limits (cf. Remark 3). Then for the next p -strip the distortion factor is already uniquely determined by the condition that the two deformed strips has to coincide along p'^*_1 , as otherwise they cannot be put together. By iteration of this argument, it can be seen that the resulting figure T'^* depends only on the single parameter d .

Reconstruction of T^* over T'^* : We start with the quad $Q'^*_{1,1}$. Without loss of generality, we can assume $V'^*_{0,0} = V^*_{0,0}$ and $V'^*_{1,0} = V^*_{1,0}$. Then we can construct the point $V^*_{0,1}$ such that its distance from $V^*_{0,0}$ equals the original length between $V_{0,0}$ and $V_{0,1}$. Note that $V^*_{0,1}$ is uniquely determined by assuming that the signatures of the slopes of the edges $V^*_{0,0}V^*_{0,1}$ and $V_{0,0}V_{0,1}$ have to agree. From the parallel condition of the edges $V^*_{0,1}V^*_{1,1}$ to $V^*_{0,0}V^*_{1,0}$ we get $V^*_{1,1}$ completing the reconstruction of $Q^*_{1,1}$, which is congruent with $Q_{1,1}$. By iteration of this process quad for quad, we can reconstruct the T -hedron T^* over T'^* . The continuous variation of the parameter d implies a continuous isometric deformation of T^* . Moreover, as T'^* has the same characteristic as T' with respect to the graphical visualization of classes done in Fig. 2, the theorem is proven. \square

Remark 3: According to [20] the flexion limits of the T -hedron are reached as soon as either a p -strip or a t -strip gets completely flat; i.e. the p/t -strip is located in a p/t -plane.

Finally, it should be noted that the smooth analogous of T -hedra are the so-called profile-affine/congruent surfaces, which are studied in [22] and more recently in [23]. A tabulated comparison of the smooth and discrete case is given in §19 of [20].

3. Parametrization of T-hedra vertices under the flexion

In order to obtain the parametrization of the T-hedron, we have to give explicit formulas for the transformations $\zeta_i := \eta_i \circ \eta_{i-1} \circ \dots \circ \eta_1$, mapping the profile curve p_0 to p_i , where the vertices are parametrized by the recursive formula $V_{i,j} = \zeta_i(V_{0,j})$. Without loss of generality, if necessary by applying a rigid transformation of the home coordinate system, one may assume that the plane π_0 , containing the profile curve $p_0: j \mapsto (V_{0,j}^x, 0, V_{0,j}^z)$, is the xz -plane and that τ_0 , the plane containing the trajectory curve $t_0: i \mapsto (V_{i,0}^x, V_{i,0}^y, 0)$ as well as the prism curve $g: i \mapsto (G_i^x, G_i^y, 0)$, is the xy -plane. Consequently, the affine transformations ζ_i preserve the z -direction and are concatenations of rotations around the z -axis, axial dilatations and translations in the xy -plane. The rotation angles $\lambda_i \in [0, 2\pi)$, the scaling factors $\mu_i \in \mathbb{R}^+$ and the translation vectors $b_i \in \mathbb{R}^2$, are determined by the trajectory curve and prism curve.

A T-hedron \mathbb{T} with vertices $V_{i,j}$ is continuously flexible in its class, if there exists a map

$$\mathbb{T}: (1 - \varepsilon_1, 1 + \varepsilon_2) \times \{0, \dots, I - 1\} \times \{0, \dots, J - 1\} \rightarrow \mathbb{R}^3, \quad (s, i, j) \mapsto V_{i,j}(s), \quad (1)$$

with $\varepsilon_1, \varepsilon_2 \in \mathbb{R}^+$, that is continuous in the first variable s and satisfies the following properties:

- For every $s \in (1 - \varepsilon_1, 1 + \varepsilon_2)$, $\mathbb{T}(s)$ is a T-hedron of the same type as $\mathbb{T} = \mathbb{T}(1)$,
- The edge lengths and interior angles of the quads $Q_{i+1,j+1}(s)$ are the same for all s .

Note that the boundary values of the interval $(1 - \varepsilon_1, 1 + \varepsilon_2)$ correspond to the flexion limits (cf. Remark 3). Due to the fact that each quad $Q_{i+1,j+1}(s)$ is a trapezoid, its shape is determined by the lengths of the four edges $p_{i,j+1}$, $p_{i+1,j+1}$, $t_{i+1,j}$, $t_{i+1,j+1}$ and (the cosine of) one interior angle $\alpha_{i,j}$; i.e.

$$\|p_{i,j+1}\|, \|p_{i+1,j+1}\|, \|t_{i+1,j}\|, \|t_{i+1,j+1}\|, \cos \alpha_{i,j} := \frac{\langle p_{i,j+1}, t_{i+1,j} \rangle}{\|p_{i,j+1}\| \|t_{i+1,j}\|}, \quad (2)$$

with $p_{i,j} := V_{i,j} - V_{i,j-1}$ and $t_{i,j} := V_{i,j} - V_{i-1,j}$, respectively. Following the proof of Section 2.3, we construct the isometric deformation of a T-hedron, by first isometrically bending the profile curve p_0 and then computing the deformation of the trajectory curve and prism curve, respectively, in such a way that the quantities of Eq. (2) are preserved. The deformation of the profile curve is then given by

$$p_0(s): j \mapsto \left(sV_{0,j}^x(1), 0, \sum_{k=1}^j n_1(k) \sqrt{\|p_{0,k}\|^2 - s^2(V_{0,k}^x(1) - V_{0,k-1}^x(1))^2} \right), \quad (3)$$

where $n_1(k) := \text{sign}(V_{0,k}^z(1) - V_{0,k-1}^z(1))$. The deformations of the prism curve and trajectory curve depend on the type of the T-hedron and are investigated in the coming subsections, where the class-preserving isometric deformations of T-hedra are briefly explained and their parametrizations are given type by type. The interested reader can find the related mathematical details in [23].

3.1. Isometric deformation of T-hedra of the first kind

Assume the trajectory curve t_0 and the profile curve p_0 in such a way that $V_{0,0}$ coincides with $(0,0,0)$. Then the parametrization of a T-hedron of the first kind, $V_{i,j}^I$, is given by:

$$V_{i,j}^I(s) := p_0(s) + t_0(s) = \begin{pmatrix} V_{0,j}^x(s) \\ 0 \\ V_{0,j}^z(s) \end{pmatrix} + \begin{pmatrix} V_{i,0}^x(s) \\ V_{i,0}^y(s) \\ 0 \end{pmatrix} = \begin{pmatrix} V_{0,j}^x(s) + V_{i,0}^x(s) \\ V_{i,0}^y(s) \\ V_{0,j}^z(s) \end{pmatrix}. \quad (4)$$

The strategy for the class-preserving isometric deformation of the aforementioned T-hedron is to deform the trajectory polygon in accordance to the deformation of the profile polygon in such a way that the quantities of Eq. (2) are preserved. From the conservation of $\cos \alpha_{i,j}$ one obtains the x -coordinates $V_{i,0}^x$ of the trajectory curve. Finally, since the information regarding the length of the trajectory is encoded

into $\|t_{i+1,j}\|$, using it will give the y-coordinates $V_{i,0}^y$ of the trajectory curve in dependence of $V_{i,0}^x$. Under consideration of $n_2(k) := \text{sign}(V_{k,0}^y(1) - V_{k-1,0}^y(1))$ the result can be summarized as follows:

$$V_{i,0}^x(s) := V_{i,0}^x(1)/s, \quad V_{i,0}^y(s) := \sum_{k=1}^i n_2(k) \sqrt{\|t_{k,0}\|^2 - \frac{1}{s^2} (V_{k-1,0}^x(1) - V_{k,0}^x(1))^2}. \quad (5)$$

3.2. Isometric deformation of T-hedra of the second kind

A T-hedron of the second kind is created by scaling and rotating a polygon around a fixed axis. Assuming the axis of this stretch-rotation to be the z-axis, the parametrization of the T-hedron of the second kind, $V_{i,j}^{II}$, is:

$$V_{i,j}^{II}(s) := \begin{pmatrix} (\prod_{k=1}^i \mu_k(s)) \cos(\sum_{k=1}^i \lambda_k(s)) V_{0,j}^x(s) \\ (\prod_{k=1}^i \mu_k(s)) \sin(\sum_{k=1}^i \lambda_k(s)) V_{0,j}^x(s) \\ V_{0,j}^z(s) \end{pmatrix}, \quad (6)$$

where $\mu_i(s) := r_i(s)/r_{i-1}(s)$ and r_i and λ_i are defined by the polar coordinates of the trajectory curve $t_0 : i \mapsto (r_i \cos(\sum_{k=1}^i \lambda_k), r_i \sin(\sum_{k=1}^i \lambda_k), 0)$.

The related class-preserving isometric deformation is obtained through manipulation of λ_i and r_i in accordance to the deformation of the profile polygon in such a way that the quantities of Eq. (2) are preserved. In fact, after deforming the profile curve, the change of r_i is obtained from the preservation of the edge length $\|p_{i,j+1}\|$. Using the conservation of $\|t_{i+1,j}\|$, $\cos \alpha_{i,j}$ and the *cosine theorem* gives the new rotation angle. The results are as follows:

$$r_i(s) := r_0(1) \sqrt{\left(\frac{r_i(1)}{r_0(1)}\right)^2 + s^2 - 1}, \quad \lambda_i(s) := \text{sign}(\lambda_i(1)) \arccos\left(\frac{r_i^2(s) + r_{i-1}^2(s) - \|t_{i,0}\|^2}{2 r_i(s) r_{i-1}(s)}\right). \quad (7)$$

3.3. Isometric deformation of T-hedra of the third kind

In the most general case, the affine maps η_i are the stretch-rotations around the points G_i . After a global translation, we can assume, that G_1 is the origin. The rotation angle λ_i is the one that is enclosed by $V_{i-1,0} G_i V_{i,0}$ and the stretching factor $\mu_i := (r_i + m_i l_i)/r_{i-1}$ is defined by the edge length $l_i := \|G_{i+1} - G_i\|$, the sign function $m_i := \text{sign}(\langle V_{i,0} - G_i, G_{i+1} - G_i \rangle)$ and by the distance between corresponding points of the prism and trajectory curve $r_i := \|G_{i+1} - V_{i,0}\|$. The vertices of the T-hedron are now parametrized by:

$$V_{i,j}(s) = \zeta_i(s) V_{0,j}(s) = R_i(s) V_{0,j}(s) + b_i(s), \quad (8)$$

where

$$R_i(s) := \begin{pmatrix} (\prod_{k=1}^i \mu_k(s)) \cos(\sum_{k=1}^i \lambda_k(s)) & -(\prod_{k=1}^i \mu_k(s)) \sin(\sum_{k=1}^i \lambda_k(s)) & 0 \\ (\prod_{k=1}^i \mu_k(s)) \sin(\sum_{k=1}^i \lambda_k(s)) & (\prod_{k=1}^i \mu_k(s)) \cos(\sum_{k=1}^i \lambda_k(s)) & 0 \\ 0 & 0 & 1 \end{pmatrix}, \quad (9)$$

$$b_i(s) := G_i(s) - \sum_{l=1}^i \prod_{k=l}^i R_k(s) (G_i(s) - G_{i-1}(s)).$$

To obtain the isometric deformation of a T-hedron of type III, we will map it to a T-hedron $\tilde{\mathbb{T}}$ of type II and then map it back to a T-hedron of type III, such that the quads of the deformed T-hedron coincide with the ones of \mathbb{T} . To this end, consider the map Φ :

$$V_{i,j} := R_i V_{0,j} + b_i \mapsto \Phi(V_{i,j}) := \tilde{V}_{i,j} := R_i V_{0,j}, \quad (10)$$

that maps \mathbb{T} of type III to $\tilde{\mathbb{T}}$ of type II, such that the rotation angles λ_i and the scaling factors μ_i are unchanged. Geometrically, $\tilde{\mathbb{T}}$ is constructed by shifting the vertical planes π_i in a parallel way, till the

new planes $\tilde{\pi}_i$ intersect in a common line over G_1 , namely, the z-axis. Corresponding edges of \mathbb{T} and $\tilde{\mathbb{T}}$ are parallel. Therefore, all the interior and dihedral angles of the quad surfaces are identical. The map Φ is surely not injective; e.g. it maps molding surfaces to surfaces of revolution. Even more, for every $\tilde{\mathbb{T}}$ of type II and a set of positive numbers $\{L_i\}$, $i = 1, \dots, I$ there exists a unique \mathbb{T} of type III, such that $\Phi(\mathbb{T}) = \tilde{\mathbb{T}}$ and the edge lengths $\|t_{i,0}\|$ of t_0 of \mathbb{T} are given by L_i . Since the dihedral angles of \mathbb{T} and $\Phi(\mathbb{T})$ are identical, the map Φ and its inverse Φ^{-1} commute with the flexion (see Fig. 4) and we can use the formulas of Section 3.2 to compute the isometric deformation of the T-hedra of type III.

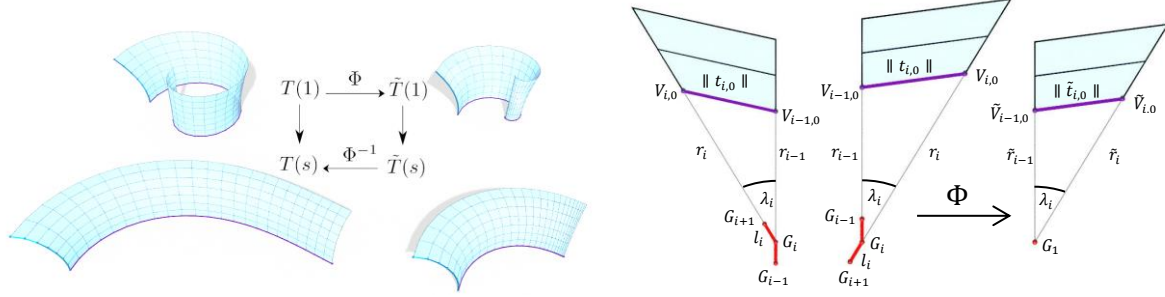


Figure 4: (left) The T-hedron $\mathbb{T}(1)$ of type III, gets first mapped to a T-hedron $\tilde{\mathbb{T}}(1)$ of type II. Then it is isometrically deformed into $\tilde{\mathbb{T}}(s)$ and then mapped back to a T-hedron $\mathbb{T}(s)$ of type III, that is isometrically equivalent to the starting surface $\mathbb{T}(1)$. (right) Illustration of a p-strip of a T-hedron of the third kind with $m_i = 1$ and $m_i = -1$, respectively, and the transformation of the latter one under the map Φ .

For a T-hedron \mathbb{T} of type III the vertices under the flexion can be computed by the following algorithm:

1. Compute the trajectory curve $\tilde{t}_0 : i \mapsto (\tilde{r}_i \cos(\sum_{k=1}^i \lambda_k), \tilde{r}_i \sin(\sum_{k=1}^i \lambda_k), 0)$ of $\tilde{\mathbb{T}} = \Phi(\mathbb{T})$ and its edge-length $\|\tilde{t}_{0,i+1}\|$ via

$$\tilde{r}_0 = r_0, \quad \tilde{r}_i = \mu_i \tilde{r}_{i-1}, \quad \|\tilde{t}_{0,i+1}\| = \|t_{0,i+1}\| \tilde{r}_i / r_i.$$
2. Deform the T-hedron $\tilde{\mathbb{T}}$ into $\tilde{\mathbb{T}}(s)$ by computing the quantities $p_0(s)$, $\tilde{r}_i(s)$, $\mu_i(s)$ and $\lambda_i(s)$, as explained in Section 3.2.
3. Compute the prism curve $g(s)$ of $\mathbb{T}(s)$ via:

$$G_1(s) = (0,0,0), \quad G_{i+1}(s) = G_i(s) + m_i l_i(s) (\cos(\sum_{k=1}^i \lambda_k(s)), \sin(\sum_{k=1}^i \lambda_k(s)), 0),$$
 with $l_i(s) = m_i(\mu_i(s) r_{i-1}(s) - r_i(s))$ and $r_i(s) = (\|t_{0,i+1}\| / \|\tilde{t}_{0,i+1}\|) \tilde{r}_i(s)$.
4. Build the isometrically deformed quad surface $\mathbb{T}(s)$, from the new prism curve $g(s)$, the profile curve $p_0(s)$ and the scaling factors $\mu_i(s)$, as explained in Eq. (8) and Eq. (9), respectively.

4. Interactive design tool for T-hedra

We provide an interactive plug-in for Rhino/Grasshopper which can be used by architects to design flexible T-hedra. This plug-in consists of three main mesh-generator components (one for each type of T-hedra) which create a T-hedron based on two boundary polygons (and a list of direction points for type III) and visualize its flexion according to the formulas presented in Section 3. In the following subsections we will explain inputs and outputs of the components, their data type and the process through the workflow (see Fig. 5).

Furthermore, we implemented the following three visualization features: The first one, which only applies for the type III component, shows tangents of the prism curve of the related molding surface in order to give the user a first idea on the initial placement of the direction points (Section 4.1). The second one is a color coding applied on quad faces, showing the proximity of the current deformation to the flexion limits (Section 4.2) and the third one is a visualization of the force transmission throughout the mesh (Section 4.3) achieved by coloring/thickening internal edges (i.e. hinges).

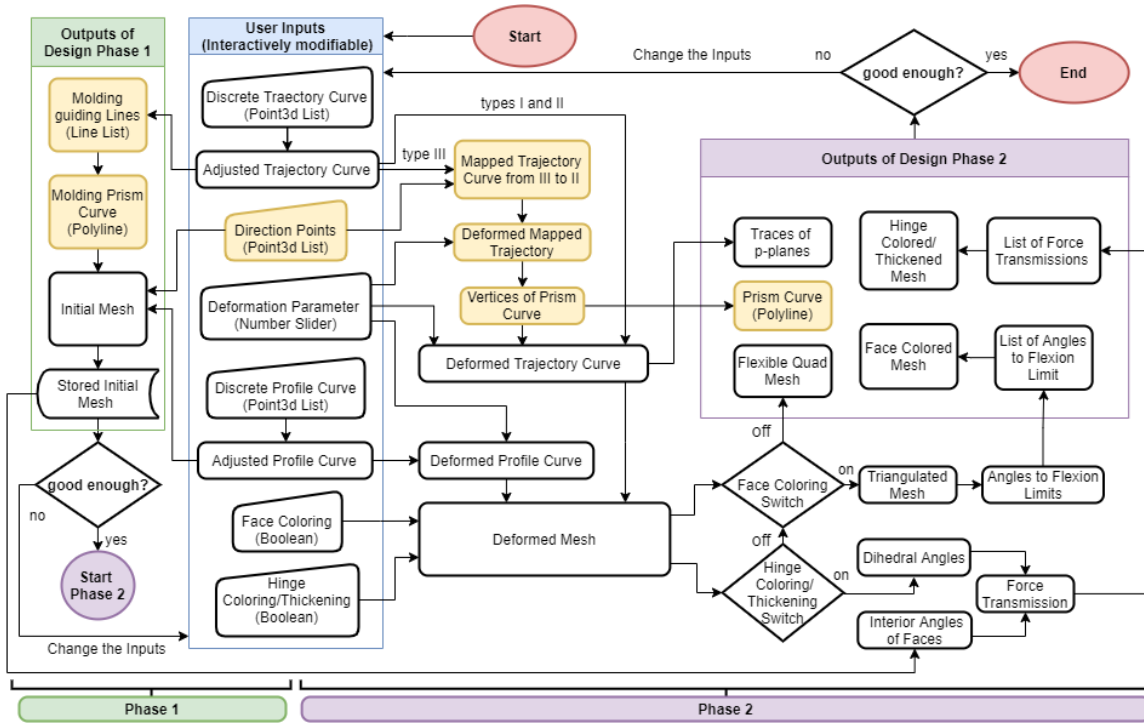


Figure 5: Flowchart of the internal process for each component of the T-hedra mesh-generator plug-in, showing all the inputs, outputs, options and features. Nodes with light yellow color are representing extra inputs, outputs and processing steps for the type III component only. The design process is carried out in two phases. In phase one an initial T-hedron (and molding guiding lines for type III) previews in the Rhino environment based on the user inputs. Once its shape is satisfying, design phase 2 can be started. Modification of the inputs in any step is always possible by simple drag-and-drops in Rhino. After the process, each component gives the designer access to several outputs beside the mesh.

Remark 4: Algorithms produced in previous sections provide an efficient implementation in such a way that the time complexity of computations for generating a flexible T-hedron with a fixed deformation parameter is $O(|V|)$.

To make the components easier to use, we have the following assumptions/constraints on the inputs:

- **Boundary polygons.** The profile polygon p_0 and the trajectory polygon t_0 should be defined as lists of points anywhere in the planes xz -plane and xy -plane, respectively. The component automatically adjusts the boundary polygons by translating these two input polygons such that they have the vertex $V_{0,0}$ on the x -axis in common, whose x -coordinate equals the one of the first point of the profile polygon.
- **Direction points.** Instead of the prism polygon for the type III component, the user can define $I - 1$ direction points, which are related to $V_{i,0}$ with $i = 1, \dots, I - 1$. Each trajectory point and its corresponding direction point specify the trace of the plane π_i carrying p_i .
- **Deformation parameter.** This parameter s can be adjusted by a number slider. The user gets a visual feedback by means of face coloring about the proximity to the flexion limits.
- **Coloring/thickening switches.** They give different options for graphical visualisation of flexion limits and force transmission throughout the mesh.

Remark 5: The components could be implemented in a way to accept other data types but since the used ones are the simplest, any other data type (e.g. polylines as boundary polygons) can be converted easily by native Grasshopper components.

4.1. On the molding T-hedron in the type III component

T-hedra of type I and II can be generated by only two boundary polygons, while a T-hedron of type III needs extra information for the direction of each p-plane. Instead of defining a prism polygon, which cannot be done in an intuitive way as its points can be located very far away from the trajectory polygon, the design process is based on a different interactive approach. Analogous to the other components, user inputs two boundary polygons and obtains the uniquely defined molding T-hedron (type III_x) together with its prism polygon g and the molding guiding lines $G_iV_{i,0}$. Now, the user has the option to place direction points on these lines to keep the molding T-hedron (see Fig. 7, right) or off the lines in the xy -plane to obtain a new T-hedron. All the resulting direction lines as well as the new prism polygon can also be shown (see Figs. 6 and 7).

4.2. Graphical visualization of the flexion limits

As a T-hedron deforms, there are two flexion limits (beside possible self-intersections), which cannot be exceeded; otherwise some hinges of a practical model will tear apart. In the general case every panel encloses different angles with the two adjacent p-planes and two equal angles with both adjacent t-planes. A flexion limit is reached if any of these angles get zero (cf. Remark 3). To visualize the closeness of a quad panel to these limits we split up the trapezoidal quad by the diagonals into four triangles, which is always possible due to its convexity. Then each angle enclosed with the adjacent p/t-planes is color-coded in the corresponding triangles of the face by using color gradients (see Figs. 6 and 7). For the top and bottom triangles of each face we use a color gradient between green ($\pi/2$) and red (zero). For the left and right triangles of each face we apply a different color gradient between white ($\pi/2$) and black (zero).

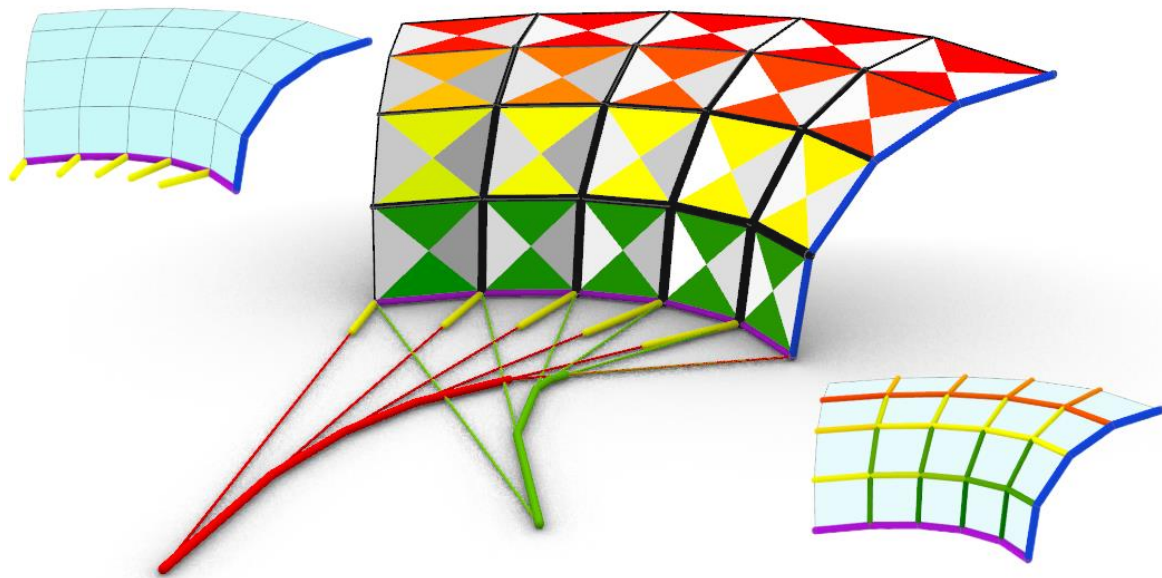


Figure 6: T-hedra generated by the type III component of the Rhino/Grasshopper mesh-generator plugin. (top left) A T-hedron generated by the profile curve (blue), trajectory curve (purple) and the direction lines (yellow). (bottom right) Visualization of the force transmission throughout the mesh by edge coloring, where the vertical hinge in the bottom right is actuated. (center) All features enabled, where the force transmission is visualized by thickening of the hinges. Moreover, the prism curve is displayed in red and the molding guiding lines as well as the related prism curve are shown in green.

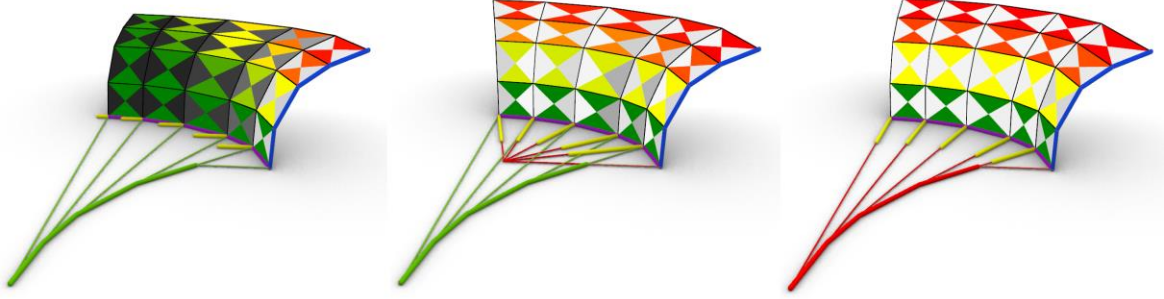


Figure 7: Demonstrating the effects of the selection of the direction points on the shapes of the resulting T-hedra with identical profile and trajectory polygons. Their shapes range from translational surfaces (with parallel direction lines; left), over T-hedra of type II (with copunctual direction lines; center) to molding surfaces (with direction lines enveloping a prism polygon; right), beside the most general case displayed in Fig. 6.

4.3. Evaluation of the force transmission characteristic

In this section we want to evaluate the force transmission throughout the polyhedral net. Note that the following considerations do not only hold for T-hedra but for all flexible quad-surfaces.

We consider the panel $Q_{i,j}$ and actuate one of its four hinges. In the following we assume the actuation of the p-hinge $p_{i,j}$ (for the t-hinge $t_{i,j}$ the procedure can be done analogously). Then we evaluate the force transmission from $Q_{i+1,j}$ to $Q_{i,j+1}$ by looking at the spherical 4-bar linkage centered in $V_{i,j}$ (see Fig. 8). According to [page 271, 24] the component of the force F , which is transmitted by the coupler link $\alpha_{i,j}$, orthogonal to the plane $Q_{i+1,j}$ (resp. $Q_{i,j+1}$) hinged by $p_{i,j}$ (resp. $t_{i,j}$) to $Q_{i,j}$ equals

$$F_{p_{i,j}} = F \cos \frac{\alpha_{i,j}}{2} \sin \delta_{i,j} \sin \chi_{i+1,j} \quad \text{and} \quad F_{t_{i,j}} = F \cos \frac{\alpha_{i,j}}{2} \sin \beta_{i,j} \sin \psi_{i,j+1}, \quad (11)$$

respectively. Elimination of F yields the following relation:

$$F_{t_{i,j}} : F_{p_{i,j}} = \sin \beta_{i,j} \sin \psi_{i,j+1} : \sin \delta_{i,j} \sin \chi_{i+1,j}. \quad (12)$$

Moreover, as our input force $F_{p_{i,j}}$ can be seen as a scaling factor we can assume that it equals 1. If we propagate the resulting force $F_{t_{i,j}}$ over the spherical 4-bar centered in $V_{i-1,j}$ from $Q_{i,j+1}$ to $Q_{i-1,j}$ we end up with

$$F_{p_{i-1,j}} = (\sin \beta_{i,j} \sin \psi_{i,j+1} \sin \gamma_{i-1,j} \sin \chi_{i-1,j}) : (\sin \delta_{i,j} \sin \chi_{i+1,j} \sin \alpha_{i-1,j} \sin \psi_{i-1,j+1}). \quad (13)$$

But beside the transmission of the force from $Q_{i+1,j}$ to $Q_{i-1,j}$ over $Q_{i,j+1}$ there exists a second one over the quad $Q_{i,j-1}$. Analogous considerations as above yield for $F_{p_{i-1,j}}$ a second value, namely

$$(\sin \gamma_{i,j-1} \sin \psi_{i,j-1} \sin \beta_{i-1,j-1} \sin \chi_{i-1,j-1}) : (\sin \alpha_{i,j-1} \sin \chi_{i+1,j-1} \sin \delta_{i-1,j-1} \sin \psi_{i-1,j-1}). \quad (14)$$

Due to §7 of [11] the expressions in Eq. (13) and Eq. (14) are identical in case of flexible quad-surfaces, which shows that $F_{p_{i-1,j}}$ is well defined. Therefore, we can use the values $F_{t_{i,j}}$ and $F_{p_{i,j}}$ as transmission index at the hinges. These values, which can be computed by iterating the above procedure over the net, depend on the selection of the actuated hinge $p_{i,j}$ or $t_{i,j}$. The obtained values are visualized by coloring/thickening the hinges (cf. Fig. 6) by mapping them between zero (red/thin) and 1 (green/thick) using the function

$$\min(|F_{e_{i,j}}|, |F_{e_{i,j}}^{-1}|) \quad \text{for } e \in \{p, t\}. \quad (15)$$

Remark 6: The inverse in Eq. (15) corresponds to the force transmission backwards through the net.

Note that until now this feature is only implemented for the edge $p_{1,1}$ as the actuated hinge.

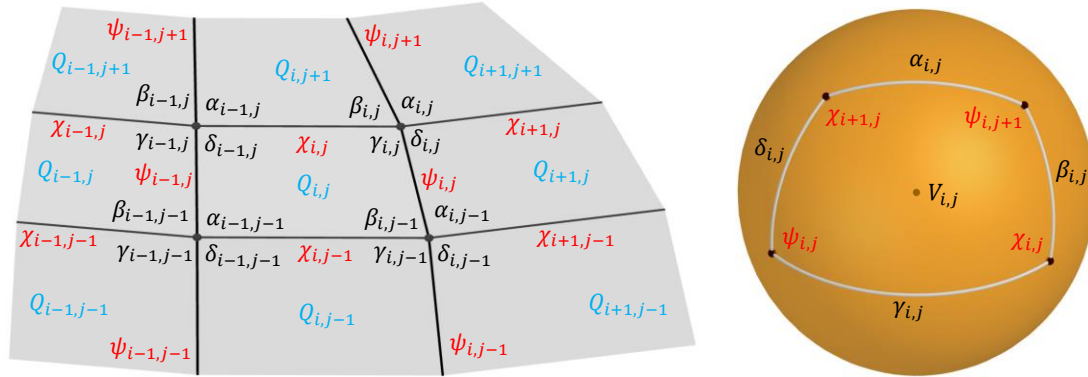


Figure 8: (left) The plane angles around the vertex $V_{i,j}$ are denoted $\alpha_{i,j}, \beta_{i,j}, \gamma_{i,j}, \delta_{i,j}$. The dihedral angles along $p_{i,j}$ and $t_{i,j}$ are denoted by $\psi_{i,j}$ and $\chi_{i,j}$, respectively, and are measured w.r.t. the same side of the T-hedron. (right) The arrangement of four panels through $V_{i,j}$ can be considered as a spherical 4-bar linkage.

5. Conclusion and future work

This paper dealt with the geometry of T-hedra, which form a special class of flexible quad-surfaces, the isometric deformation of all their subclasses in terms of a recursive parametrization of their vertices and the implementation of a Rhino/Grasshopper mesh-generator plug-in for designing them.

Concerning theoretical investigations, one of the future works is to adapt formulas and accordingly the algorithms in order to unify all three components, which will allow further freedom in the design of T-hedra and will be carried out in the next version of the plug-in. Furthermore, we plan to implement more interactive features; e.g. we want to provide the user the possibility to select the actuated hinge to investigate its influence on the force transmission throughout the mesh. Moreover, the user can select the (grounded/fixed) face to which the mesh deforms relatively. This will also influence the shape of the related swept volume, which we plan to visualize, taking the flexion limits as well as the avoidance of self-collisions into account.

Acknowledgements

The research is supported by grant F77 (SFB “Advanced Computational Design”, subproject SP7) of the Austrian Science Fund FWF. The first author wants to thank Florian Rist, Stefan Pillwein and Mojtaba Ghorbanalibeik for their support concerning the implementation of the Rhino/Grasshopper plug-in.

References

- [1] Hoberman Associates Inc. <https://www.hoberman.com>, Accessed: March, 31, 2021.
- [2] Schumacher M., Schaeffer O. and Vogt M.-M., *move – Architecture in Motion*. Birkhäuser, 2009. doi: <https://doi.org/10.1515/9783034608541>.
- [3] Zheng C., Sun T. and Chen X., Deployable 3D Linkages with Collision Avoidance. *Proceedings of the ACM SIGGRAPH/Eurographics Symposium on Computer Animation*, 2016, 179-188. doi: <https://doi.org/10.2312/sca.20161235>.
- [4] Overvelde J.T.B., Weaver J.C., Hoberman C. and Bertoldi K., Rational design of reconfigurable prismatic architected materials. *Nature*, 2017; **541**; 347-352. doi: <https://doi.org/10.1038/nature20824>.
- [5] Konakovic-Lukovic M., Panetta J., Crane K. and Pauly M., Rapid Deployment of Curved Surfaces via Programmable Auxetics. *ACM Transactions on Graphics*, 2018; **37.4**; 1-13. doi: <https://doi.org/10.1145/3197517.3201373>.

- [6] Pottmann H., Eigensatz M., Vaxman A. and Wallner J., Architectural Geometry. *Computers and Graphics*, 2015; **47**; 145-164. doi: <https://doi.org/10.1016/j.cag.2014.11.002>.
- [7] Barozzi M., Liemhard J., Zanelli A. and Monticelli C., The sustainability of adaptive envelopes: developments of kinetic architecture. *Procedia Engineering*, 2016; **155**; 275-284. doi: <https://doi.org/10.1016/j.proeng.2016.08.029>.
- [8] Soru M. (2014) A spatial kinetic structure applied to an active acoustic ceiling for a multipurpose theatre. *Master thesis, Delft University of Technology*.
- [9] Thün G., Velikov K., Ripley C. and Sauve L., McGee W., Soundspheres: Resonant Chamber. *ACM SIGGRAPH, Art Gallery*, 2012; 348-357. doi: <https://doi.org/10.1145/2341931.2341936>.
- [10] Bobenko A.I., Hoffmann T. and Schief W.K., On the integrability of infinitesimal and finite deformations of polyhedral surfaces, in *Oberwolfach Seminars, Discrete Differential Geometry* A.I. Bobenko et al. (eds.), 2008, 38:67–93. doi: https://doi.org/10.1007/978-3-7643-8621-4_4.
- [11] Kokotsakis A., Über bewegliche Polyeder. *Mathematische Annalen*, 1932; **107**; 627-647. doi: <https://doi.org/10.1007/BF01448912>.
- [12] Stachel H., A kinematic approach to Kokotsakis meshes. *Computer Aided Geometric Design*, 2010; **27**; 428-437. doi: <https://doi.org/10.1016/j.cagd.2010.05.002>.
- [13] Nawratil G., Reducible compositions of spherical four-bar linkages with a spherical coupler component. *Mechanism and Machine Theory*, 2011; **46.5**; 725-742. doi: <https://doi.org/10.1016/j.mechmachtheory.2010.12.004>.
- [14] Nawratil G., Reducible compositions of spherical four-bar linkages without a spherical coupler component. *Mechanism and Machine Theory*, 2012; **49**; 87-103. doi: <https://doi.org/10.1016/j.mechmachtheory.2011.11.003>.
- [15] Nawratil G. and Stachel H., Composition of spherical four-bar-mechanisms. *New Trends in Mechanisms Science – Analysis and Design*, D. Pisla et al. (eds.), Springer, 2010, 99-106. doi: https://doi.org/10.1007/978-90-481-9689-0_12.
- [16] Izmistiev I., Classification of flexible Kokotsakis polyhedra with quadrangular base. *International Mathematics Research Notices*, 2017; **3**; 715-808. doi: <https://doi.org/10.1093/imrn/rnw055>.
- [17] Erofeev I., Ivanov, G., Orthodiagonal anti-involutive Kokotsakis polyhedra. *Mechanism and Machine Theory*. 2020; **146**; 103713. doi: <https://doi.org/10.1016/j.mechmachtheory.2019.103713>.
- [18] Tachi T., Generalization of rigid foldable quadrilateral mesh origami. *Journal of the International Association for Shell and Spatial Structures*, 2009; **50.3**; 173-179.
- [19] Tachi T., Freeform Rigid-Foldable Structure using Bidirectionally Flat-Foldable Planar Quadrilateral Mesh. *Advances in Architectural Geometry*, 2010; **14**; 203-115. doi: https://doi.org/10.1007/978-3-7091-0309-8_6.
- [20] Sauer R. and Graf H., Über Flächenverbiegung in Analogie zur Verknickung offener Facettenfläche. *Mathematische Annalen*, 1931; **105**; 499-535. doi: <https://doi.org/10.1007/BF01455828>.
- [21] Online catalogue of the collection of kinematic models at the Institute of Discrete Mathematics and Geometry, TU Wien. <https://www.geometrie.tuwien.ac.at/kinmodelle>, Accessed: March, 31, 2021.
- [22] Sauer R., *Differenzgeometrie*. Springer, 1970.
- [23] Rasoulzadeh A. and Tervooren, J., A Study on the Class-Preserving Isometric Deformations of T-surfaces, (*in preparation*).
- [24] Chiang C.H., *Kinematics of Spherical Mechanisms. Volume 5*. Cambridge University Press, 1988.